Desertification in Arid Colorado Shortgrass Steppe? Fast Fourier Transform and Autocorrelation Function Analysis of Emerging Periodic Vegetation Patterns

A Thesis
Presented to
The Environmental Studies Program
Colorado College

By
Amelia McDonald
April 2023

Abstract

The spatial organization of an ecosystem speaks to the environmental conditions and intrinsic qualities of the organisms present. This is because extrinsic factors, such as climate, apply stressors on organisms that respond by spatially organizing in a way that best suits their needs for survival. At Chico Basin Ranch, Colorado, the blue grama grasses visually show spatial patterning, with stripes of vegetation alternating with stripes of bare ground oriented horizontally along hillslope. This pattern is likely driven by short range facilitation, where plants facilitate their own growth by improving their growing conditions via increased surface water infiltration, and long-range inhibition, where growing conditions away from the densely vegetated patch are made inhabitable by the population inside the vegetation patch. These patterns likely formed as a response to increasing aridity in Colorado, which is limiting water. Limited water encourages plants to reorganize in order to persist under more challenging conditions. However, periodic patterning can be an early warning sign that a vegetated landscape may succumb to desertification. Understanding if a landscape is patterned periodically is important in informing conservation efforts to prevent desertification.

In order to determine if the patterning visible at Chico Basin Ranch is periodic and statistically significant, we used a 2-Dimensional Fast Fourier Transform (FFT) and the Autocorrelation Function (ACF). We applied FFT and ACF to datasets derived from aerial imaging from Google Earth for the years 2019, 2017, 2005, and 2003 of our AOI at three different scales using a custom-build code in R and the software PaSSAGE 2. Through this analysis, we were able to determine the presence and details of spatial patterning for the years examined. FFT and ACF analysis for the year 2019 showed distinct periodic patterning with waves ranging from 15-20 meters in the NW-SE direction. The analysis of 2017 showed congruence between ACF and FFT with similar results to 2019, meaning it detected periodicity with the same directionality and frequency. In contrast, the results from 2005 and 2003 both show incongruencies between methods of analysis, and our methods did not detect any significant periodic patterning. We interpreted these years as displaying some patchy spatial organization, however there is little to no periodicity, unlike the years 2017 and 2019. This leads us to conclude that there has been an emergence of periodic patterning in the population of blue grama at Chico Basin Ranch between the time periods of 2003-2005 and 2017-2019. These results are congruent with the significant decrease in blue grama at the Chemical Depot in Pueblo, 30 km south of our field site, which additionally confirms co-occurring changes in climate with increasing aridity and decreasing precipitation over the course of the study (Rondeau, 2016).

Intro

Periodicity commonly occurs in nature when looking at the patterned spatial organization of organisms across landscapes. For example, in the Rocky Mountains, ribbon patterns of Engelman spruce at tree line form a striking pattern (Malanson et al., 2011). Across the country in the freshwater marshes

of Maine, the tussock sedge grows in regularly spaced clumps (Rietkerk, 2008). Patterns of organization can be characterized as isotropic, meaning individuals are spaced symmetrically horizontally and vertically, or anisotropic, whereby individuals are spaced symmetrically only in one direction. Both isotropic and anisotropic periodic patterns exist across a variety of ecosystems, each with their own unique set of drivers that form and maintain their organization (Rietkerk, 2008). The anisotropic pattern of spruce at tree line are caused by interactions between wind and snow which inhibit growth through accumulation of snow between populations of trees, whereas the anisotropic pattern of the tussock sedge is related to the dead littler that the plants produce, shading their neighbors at regular intervals in all directions (Rietkerk, 2008).

The mechanisms that drive periodic patterns in nature, such as those mentioned above, include the positive feedbacks of short-range facilitation and long-range inhibition that occur simultaneously (Rietkerk, 2008). When facilitation occurs on a short scale and inhibition occurs at a long distance, patterns will likely form and remain in the system while feedbacks are in play. In general, these feedbacks result as a response to environmental stressors in the system, that in turn can support a landscape composed of both vegetated and non-vegetated areas, maximizing the acquisition of limiting resources. It is important to understand the role of these scale-dependent feedbacks in driving the stability and diversity of ecosystems.

Positive feedbacks in the form of short-range facilitation assists in the formation and maintenance of periodic patterning in nature by allowing populations to support their own growth within short distances. By improving the populations' ability to persist within their immediate vicinity, especially when environmental stressors make resources more limited, this feedback maintains growth and survival of the population (Scheffer et al. 2003). Therefore, we can consider this positive feedback to be a resource driven response. An example of short distance facilitation can be seen in mussel beds; Mussel beds in the sediments of the Wadden Sea in the Netherlands are arranged in a regularly striped pattern perpendicular to the tidal flow. The literature suggests that this is the result of scale-dependent feedbacks. Conspecifics are the main source of substrate when located in a sediment rich environment that does not allow attachment directly to the ocean floor. This indicates that they facilitate their own growth on a short scale by providing each other substrate for attachment (Rietkerk 2008).

However, short scale facilitation would not be enough alone to develop patterning in the mussel beds. Negative feedbacks on a long scale are necessary for the formation of periodic patterns, whereas positive feedback contributes to the sharpening of boundaries between patches (Rietkerk, 2004). The feedback supporting inhibition acts to prevent growth or survival of future organisms at threshold distances from the population. This produces an inhospitable area between patches, creating a pattern that can be periodic (Sheffer, 2001). When looking at the case study of mussels in the Wadden Sea, the population of mussels would remain evenly spaced, rather than form patterns. The pattern formation that results from long distance inhibition allows for the facilitation from conspecific substrate for attachment, while also allowing proper water flow to bring sufficient algae. Competition over algae would occur if water flow was decreased by a contiguous population of mussels. Gaps running

perpendicular to the tidal flow resulting from this long-distance inhibition promote a tidal flow rich enough in algae to support the population (Rietkerk, 2008).

Another ecosystem that is more commonly associated with scale-dependent feedbacks is arid grassland. Arid grasslands are notoriously resource limited ecosystems, with water being the most scarce. Therefore, in some cases, vegetation self organizes into periodic patterns in order to concentrate resources, such as water and nutrients, and maximize water retention (Dunkerly 2018). Patterns may vary spatially, taking many shapes including labyrinths or spots. Additionally, they often take the shape of vegetation bands or stripes that are oriented across the slope with bands of bare land in between patches. This activates a runoff-runon system which is dependent on vegetation density and infiltration (Ludwig et al. 1998). In this system, there is strong positive feedback between vegetation density and infiltration, which supports the run-on component of this process. Dense patches of vegetation are better able to infiltrate water than homogenous landscapes due to the influence of root structures on soil structure.

By permeating dense soils, roots add micropores and channels in which water may flow. This prevents runoff and directly drives water towards root systems, greatly increasing the water retention for the vegetation patches (Dunkery, 2018). Additionally, vegetation cover itself aids in water retention of soils. Evaporation level, which corresponds directly to temperature, wind, and humidity deficits, is very high in arid grassland ecosystems. Vegetation cover can minimize evaporation from soils by cooling the surface temperature down by shading out incoming radiation (Noy-Meir, 1973). Dense vegetation cover also protects soil against wind, further reducing water loss through evaporation (Noy-Meir, 1973). Unlike these patterned landscapes, homogenous landscapes may not be able to support high levels of infiltration and run-on. This is because of the dispersed nature of homogeneous landscapes, which limits water infiltration due to a lack of dense root structures, cooling via shading of soil, or wind protection. Therefore, patches of dense vegetation alternating with bare patches are more resource efficient than homogenous landscapes.

The mechanism that can drive periodic vegetation patterning when paired with short-range facilitation is long-range inhibition. In arid grasslands, inhibition at a threshold distance from the initial populations of vegetation occurs when the infiltration of the direct rainfall is not enough to sustain vegetation cover and the vegetation needs water subsidy from uphill. Thus, the system no longer supports the lower vegetation, and bare ground becomes the new state in these areas (Dunkerley, 2018). Additionally, shallow root systems spread horizontally from vegetative patches. This depletes water availability further from the patch, preventing the survival of preexisting vegetation or the regrowth of seedlings at a distance (Mayor, 2013). Without the ability to support vegetation, the bare ground will replace the vegetation, forming a crust (Dunkerley, 2018). Soil crusts are impermeable both to root structures and to rainfall. Without precipitation being able to infiltrate through the soil crusts, the water concentrates and runs off the bare patches. Downhill patches harvests this concentrated flow of water, acting as a runoff sink. The increased amount of water that runoff delivers to downslope patches is the result of long-range inhibition and is the primary driver for the formation and maintenance of this spatial pattern (Rietkerk et al, 2008).

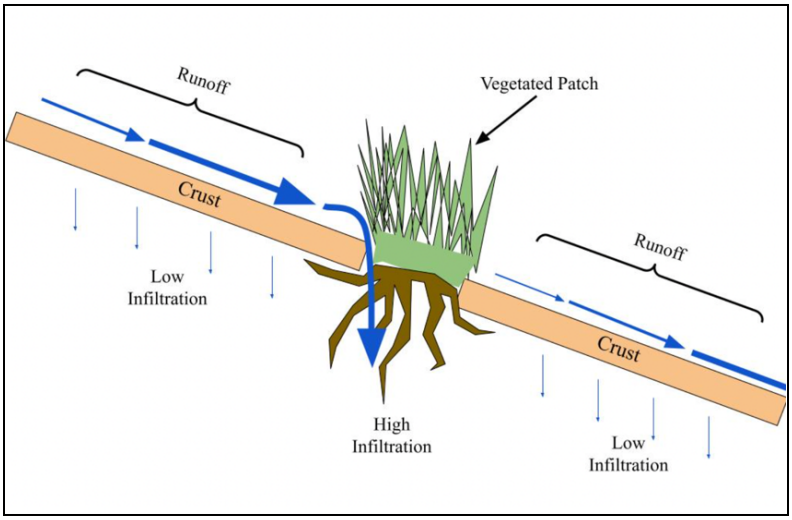

Figure 1. Runoff – runon system occurring in patchy grassland ecosystems (Foster et al. 2021)

Patterns driven by short range facilitation and long-range inhibition, such as those in arid grassland ecosystems, indicate that the environment may have bistable states. Bistable states, or bistability, is the landscape's ability to support two alternate states within the same range of environmental conditions, dependent on the initial starting state (Dale et al 2014). Arid grasslands can be dominated by either vegetation or desert scrub, which is partially bare with a cover of cactus, under the same range of temperatures, precipitation, humidity deficits, and wind conditions. The resulting state is dependent on the vegetation density it begins with. Vegetation patterns result as environmental conditions become less favorable for the vegetated state. By stressing the existing population of vegetation, increasingly arid conditions push the stable state towards the alternate state of degradation by forming an intermediate patterned state. Patterning forms to slow the degradation of the landscape to prevent full state change, but as poor environmental conditions progress, the resilience of the ecosystem decreases. In this study, we define resilience as the amount of pressure the ecosystem can withstand without fully shifting states (Mayor, 2013).

While the formation of patterning may be a smooth transition, it is possible for the smooth change to suddenly shift into the contrasting state. This switch can be represented by a catastrophic bifurcation curve which folds over on itself, in a backwards Z shape (Figure 2). When the ecosystem is in the state of the upper branch, it cannot move easily to the bottom branch. This is where patterning occurs. When conditions change just enough to pass the threshold ('saddle-node' or 'bifurcation' point), a quick shift to the bottom branch occurs. There is no significant difference in the amount of change needed to push the environment over the edge from which the previous change had occurred. This makes the bifurcation difficult to predict. Unfortunately, it is hard to reverse bifurcation because conditions cannot simply be restored to the level before the change (Scheffer, 2003).

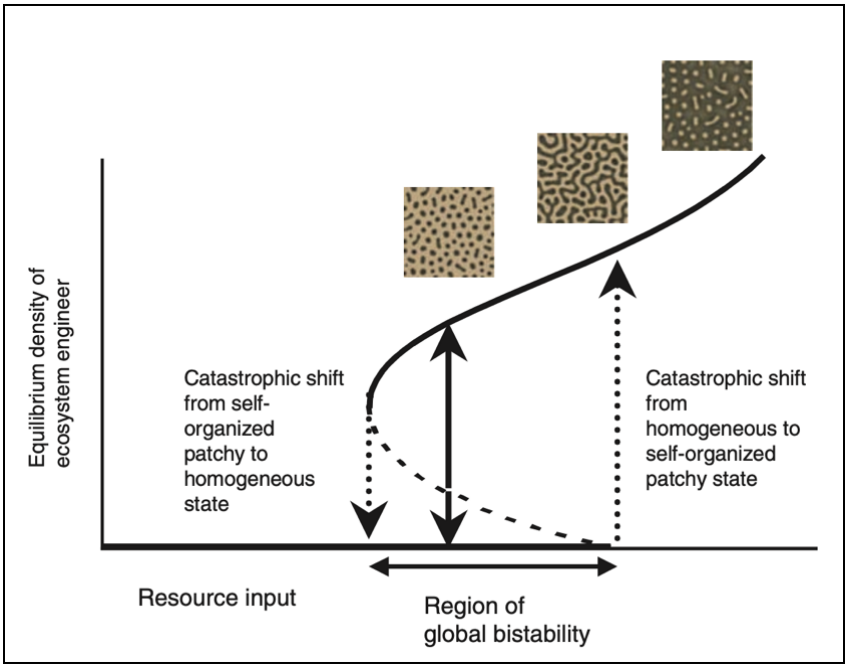

Figure 2. Catastrophic curve indicating levels of bistability that will support multiple vegetation states or cause catastrophic shifts (Rietkerk et al., 2004)

The conditions for degradation and recovery do not overlap like the initial conditions that could support both states. Therefore, it is much more difficult to reverse. In other words, decreasing the perturbation to the level it was at before bifurcation occurred, by increasing water availability for example, will not restore the ecosystem. The phenomenon that describes how some spatial structures can only change when resources decrease, and not when they increase, is called hysteresis. Hysteresis makes the reversal of desertification incredibly hard to achieve and stresses the importance of preventing bifurcation from occurring in the first place to preserve vegetation (Rietkerk 2004). In order to understand the resilience of an arid grassland ecosystem for restoration efforts, patterns that indicate stressed ecosystems must be examined.

Patterns may not always indicate a stressed ecosystem, and sometimes, we can clearly see patterns in our daily lives. Seasons progress from spring, to summer, to winter, to fall, and back again. However, periodic waves that make up the spatial organization of systems can be quite complex, despite what theoretical models might otherwise indicate. An example of a system that is composed of complex waves are the sounds made when someone plays a chord on a guitar. Sound results from the pressure waves formed when someone plays the chord. However, the sound produced by the waves is not a single sound. Each string contributes to the specific wave produced, and therefore the sound that we hear. Therefore, the wave produced by the chord is the sum of each of the single strings with their own unique waves. A trained musician can tell which notes constitute the chord, though generally it sounds like one complex note.

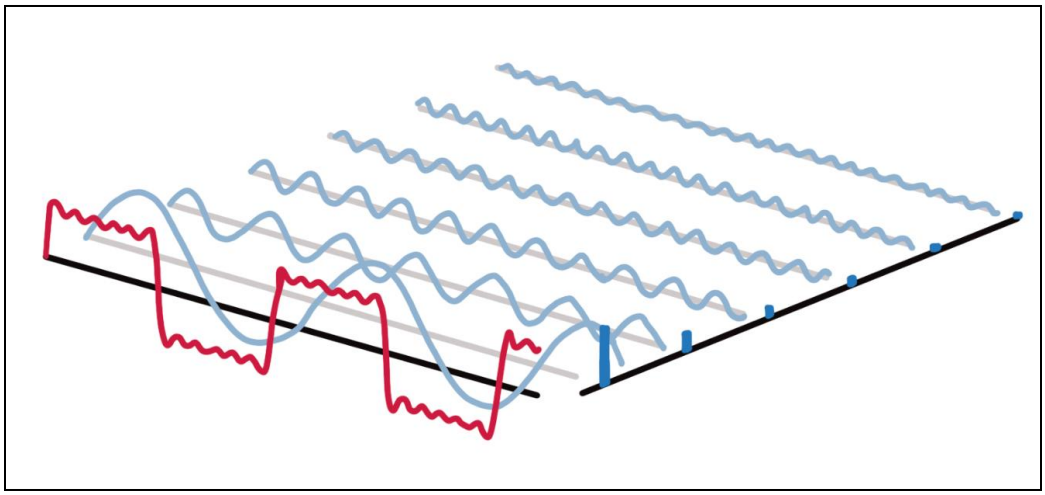

Figure 3. Composition of simple waves making up a complex wave

In nature, it can be more difficult to detect the simple wave components of a complex wave. Though, as Fourier discovered, no matter how complicated a periodic wave may appear, it is always the sum of many simple waves (Penny 2013). So, much like the pressure waves formed in the air when a chord on a guitar is played, waves in nature are simply the composition of many simple waves. Fast Fourier Transform (FFT) is one method of analysis of complex waves. FFT can simplify the waves within the spatial system by determining the individual periodic waves that together compose the complex wave. Its outputs can include the most dominant simple waves, their strength, the angle at which they occur, and the number of oscillations (Penny, 2013). However, FFT is not always able to accurately measure periodicity when the spatial extent it is applied to does not capture enough oscillations for us to consider the wave periodic (Penny, 2013).

It is important to use additional methods to examine periodicity in spatial patterns. Congruence between multiple methods of analysis increases certainty in the results to best inform restoration strategies. The Autocorrelation Function (ACF) is a tool that, used in conjunction with FFT, can inform the periodicity of patterns. ACF determines spatial correlation, which is how correlated points or polygons are on a scale of time or distance (Dale et al 2014). When the two points next to each other have similar value for their attribute (e.g. similar vegetation cover), spatial autocorrelation will be positive and high. If the value of the attribute for neighboring points is not related, the autocorrelation will be close to zero. When the value of the attribute of the neighboring points is opposite, the autocorrelation will be negative 1. For example, at points with high vegetation cover that have neighboring points that have low vegetation cover, the spatial autocorrelation will be negative. However, in patchy systems where the patches do not show any degree of spatial organization or regularity, autocorrelation decreases with distance (Dale et al., 2014).

Periodic patterns, repeating consistently with the same wavelengths, amplitudes, and frequency, are easy to measure using ACF. This is because correlation can be measured for the peaks and troughs of the patterns and will be shown as the alternation of positive and negative correlation. If the reference point

is the peak of the wave, all future peaks should be highly correlated, and all troughs should be negative. When looking at vegetation patterns, a band of dense vegetation would be negatively correlated to the band of bare ground neighboring it, and highly correlated with the next patch of grass occurring at a set distance. This clear repetition, or lack thereof, in analysis of a wave through ACF is a clear indicator of periodicity in a wave (Dale et al 2014).

This study aims to detect periodicity in vegetation patterns at Chico Basin Ranch. Our hope is that by studying the emergence of periodic patterns at Chico Basin, we will be able to better to predict a state change to bare land and inform conservation efforts in preventing bifurcation from occurring. Chico Basin Ranch, located 30 miles east of Colorado Springs, is an arid grassland ecosystem. The dominant vegetation type in this study site is blue grama, a shallow rooted shrub grass. The literature considers blue grama to be fairly drought and grazing tolerant, though it relies heavily on rainfall during its growing season, which occurs from April through September (Randeau et al, 2016). According to a study conducted through Colorado State University, blue grama has been in decline since 2002 at a site with similar elevation, climate, and ecosystem type as our study site 30km south (Rondeau, 2016). 2002 was a major drought year in which blue grama was unable to produce new growth and their mortality was above average. Throughout the length of their study, from 1999 to 2015, the blue grama population declined by 50%. This large decline persisted despite the high precipitation levels during 2014 and 2015, which indicates that a few years of adequate rainfall cannot simply reverse years of drought conditions (Randeau et al, 2016).

Based on visual inspection, vegetation patterns have emerged at Chico Basin Ranch in the same timeframe as the nearby site in Pueblo experienced precipitous decline in blue gramma vegetation cover. Similar decline in blue grama may have occurred at our field site because bare patches of ground show dead and disintegrating root crowns of blue grama. In this study, we aim to use FFT and the ACF to determine the strength and directionality of the periodic patterning of blue grama that has resulted from overall decline. Our goal is to find congruence between FFT and Autocorrelation to come to a more concrete conclusion about the prevalence of periodic patterning in this ecosystem. This will inform future conservation efforts in shortgrass desert steppe.

Methods

Field site and Data Collection

Our study was conducted at 1564 meters above sea level at the Chico basin ranch in the south plains of central colorado. This area is an arid grassland ecosystem dominated by blue grama and bare ground. Other prominent species include buffalo grass, needle and thread grass, cholla cactus, and opuntia cactus. Our area of interest (AOI), located in a pasture east of the local landing strip, displays patterning that appears to be periodic based on visual inspection. To confirm this hypothesis, we conducted an in-depth analysis on the spatial organization of the system. We performed our analysis for the range of years from 1999 to 2020, specifically choosing the years 2003, 2005, 2017, and 2019 for our analysis to represent the beginning and end of our date range. For these years, we collected Google Earth aerial imagery with a spatial resolution of 0.25-meters. After obtaining the raw imagery, we

prepared the data sets in ArcGIS Pro by resampling images to 0.5-meter pixels. The images were set to a grayscale gradient, with values representing vegetation density, where dark pixels represent high values of vegetation density and light pixels indicated low to no vegetation density. We clipped the image into 100-meter by 100-meter squares, which we then divided into 50 by 50 meter and 25 by 25 meter squares to ensure that our data was at the right spatial extent to analyze.

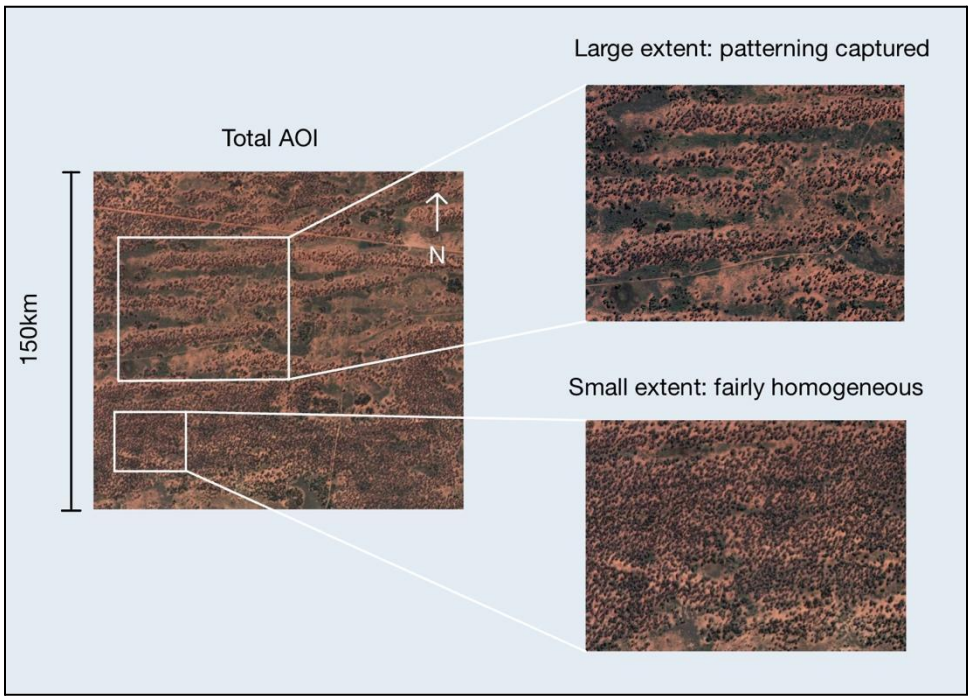

Figure 4. Example of the effect of scale in identifying landscape organizational arrangements

Google Earth Imagery from Australia at -32°, 142°

We heavily considered scale, defined as spatial extent, when running our analysis because the size of the area we were analyzing influences the results of both FFT and ACF, our two methods of analysis. This is because identifying dominant spatial patterns is dependent on the scale of analysis. For patterns generated mathematically, the scale is less relevant, as we can generate the pattern for any given dimension. As long as the scale of the analysis is larger than the wavelength of the pattern, the pattern will remain fixed. Other researchers have also noted this phenomenon in the literature when mathematical models predict perfect periodicity for a landscape's spatial organization (Penny et al, 2013). However, extrinsic factors influence real life ecosystems through small-scale interactions that result in inherent disorder of patterns (Penny et al. 2013). One major factor is hillslopes' orientation and variation over a landscape, which influences the direction, frequency, and periodicity of a pattern. Therefore, we expect the pattern in a real ecosystem to vary in wavelength and orientation across space in response to the variation in the underlying factors. A scale that examines an AOI with too many geographic variations due to its large size, for example, will be unable to identify a significant pattern. A

smaller scale study may be able to identify the dominant pattern of a specific area, whereas a larger extent would lose the spatial organization. However, if the scale is too small, it may only capture a portion of the pattern which would also result in the analysis losing the wave as well. Therefore, we examined two scales or spatial extents in our study to account for the inherent variations in natural systems.

FFT

Fourier's discovery that all complex waves are conceptualized and analyzed as the sum of simple periodic waves is integral in the analysis of this landscape. Fast Fourier Transform can detect the dominant simple wavelengths and amplitudes that, added together, form the complex wave observed in the field data. FFT achieves this by multiplying the function of the complex wave in the data by a series of sin and cos waves of different frequencies. The waves multiplied by the complex wave in the field data are called "fishing waves," as they are fishing for signals in the complex wave. The results are based on the integration of the area under the curve for the product of the sin and cosign fishing waves and the complex wave from our field data. When the resulting area under the integrated curve is positive, there is a signal from the simple wave corresponding to the multiplicative function. This means that the simple wave is present in the complex wave from our field data. If a simple fishing wave does not resonate with the complex field wave, the area under the curve for the resulting multiplied wave is zero. This is because the sum of the negative values of the curve are equal to the sum of the positive values (Transnational College of Lex, 1995).

2-Dimensional FFT

Typically, researchers in the field cite using FFT when looking at a complex wave propagating through time, like a sound wave from playing a chord on the guitar. In our study, we are looking at waves that are moving spatially across a landscape. Due to the spatial nature of our study, we must include the directionality of waves that form these spatially organized systems. Therefore, using Two-Dimensional FFT was more appropriate for the study than the more commonly used One Dimensional FFT. The code used to conduct the 2D FFT analysis, co-written by Miro Kummel and Amelia McDonald in R (Appendix X), gives us a matrix of the underlying values necessary to construct a periodogram. Periodograms are figures that we use to identify dominant frequencies which are the simple waves that make up the complex spatial structure (Renshaw et al, 1983). Periodograms visually display their qualities, including direction, frequency, and magnitude (amplitude). A pair of dots that are symmetrical around the 0,0 position in the center of the periodogram represent each simple wave. The distance of the dots from the center corresponds to the frequency, or more specifically wave number, of the corresponding wave. Connecting the dots representing dominant wavelengths across the center point creates a line of an angle corresponding to the direction of the wave. The pixel value of the dots in the periodogram corresponds to the amplitude of the wave. We report amplitude as the proportion of variance in the image that the wave explains. The statistical significance of individual waves in the periodogram is determined using a modified chi-square distribution (Renshaw and Ford, 1984).

The periodograms from our analysis (Figures 5 and 6) display all simple waves that make up our data set. For our study, we determined which three simple waves are the most dominant by identifying the three waves with the highest pixel values in the corresponding periodogram. These dominant waves are responsible for, and explain, the largest amount of variance in the original image. Then, we summarize the information in the periodograms by using an angular and a radial spectrum. Angular spectra take equal angle slices of the periodograms. The signals aggregated in each slice are represented by peaks on the corresponding graph, with peak height indicating the aggregated signal of waves present at each angle. This information then dictates the direction of the incoming waves Radial Spectrums divide the periodograms into rings or bands of equal frequency, resulting in what looks like tree rings. The peaks on the corresponding graph represent bands where waves are aggregated, the aggregated signal of waves shown by peak height.

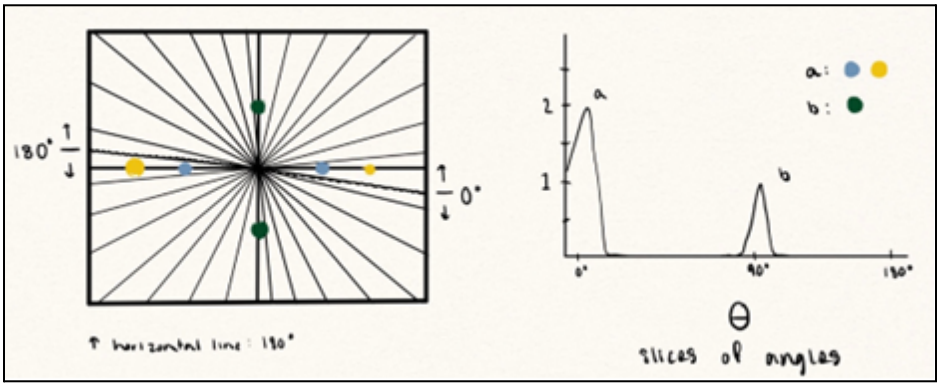

Figure 5. Example of an Angular Spectra

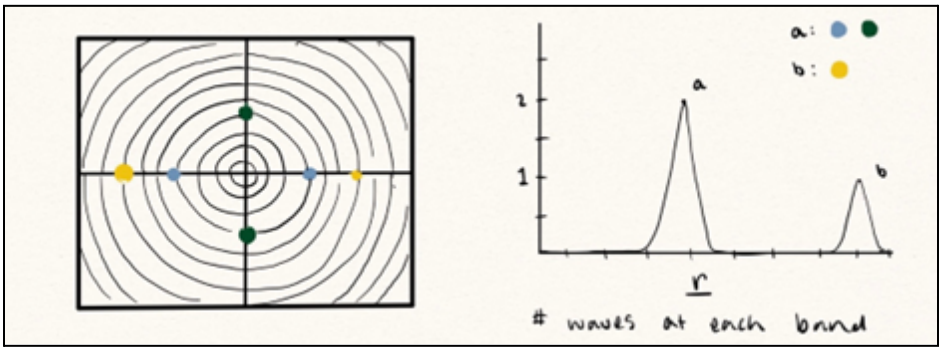

Figure 6. Example of a Radial Spectra

After producing these outputs, we then randomized the datasets to test whether the observed radial and angular spectra differ statistically significantly from complete spatial randomness. To randomize the dataset in R, we shuffled the existing values into a new order, comparable to a TV when the screen breaks and pixels no longer show a clear picture, but random pixels covering the screen. We conducted the randomization on the original black and white photos of our AOI. The completely unorganized dataset represents a homogeneous ecosystem with no spatial structure. This is a method commonly used in studies of spatial organization. Randomizing, or scrambling, data gives a useful

comparison of the results of FFT. In our study, randomization demonstrated what the waves in our landscape would look like if there was no spatial organization.

The randomizations produced a range of expected values in the radial and angular spectra based on the assumption of complete spatial randomness (CSR). To achieve this, we applied a 2D FFT analysis to the randomized dataset, including the calculation of the angular and radial spectra. We repeated This procedure 1000 times and the plotted line for each FFT randomization resulted in the graph for the angular and radial spectra of the real image. This results in our final graphs displaying a band of results from the spectra that represent what can be expected from complete spatial randomness. Any real spectra that deviated from the band of randomized values are deemed statistically significant and provide a clear visual of significant values from the data that lie outside of random spatial arrangement.

An additional factor we considered when analyzing spatial organization from our dataset using the radial spectra was the wave frequency, parameterized here as the wave number (number of waves per length of the side of the square AOI). For a wave to be considered periodic, it must meet a defined threshold number of oscillations. If the wave only completes one or two oscillations in the AOI, it is unclear if the pattern will continue to repeat itself outside of the AOI, or if it just represents a patchy non-periodic distribution of vegetation. Consequently, the wave cannot be identified as periodic if it repeats only once or twice. While there is no clear consensus in the literature on the most accurate threshold of wave number for periodicity, we followed recommendations by Penny et al (2004) and decided that if a wave oscillates four times over the distance of our AOI, we could reasonably assign the wave to be periodic. Waves that had wave numbers lower than 4 were interpreted as signifying that the spatial organization of vegetation at this scale is patchy, but not oscillatory or periodic. Alternative interpretation of waves with wave number less than 4 is that the spatial organization is periodic, but over a wider scale than our study accounted for. This points to the importance that scale has on the results of our study.

ACF

We can calculate the Autocorrelation Function for spatial data organized as points or polygons that have specific attributes. In the case of our study, the attribute we are considering is density of vegetation. We organized our data as pixels, which can be thought of as points with x , y coordinates for the center of each pixel. ACF determines if the vegetation density at the point of interest predicts the vegetation density at neighboring points or polygons. For polygons, correlations can be made for immediate, or first-degree neighbors, second degree neighbors, third degree neighbors, and so on for the extent of the dataset. For data organized as points, correlations can be made for points within different distance bands. For systems with two dimensions, such as the complex waves in our dataset, the autocorrelation function can be made for different directions. The neighboring sets for which we performed a two-dimensional analysis on are defined both by distance and direction. This allows us to study how autocorrelation varies across space for all directions in our AOI.

We calculated spatial autocorrelation using Moran's I. The reason that we cannot perform simple correlations is because each focal polygon or point has several neighbors. We must first aggregate the

disparate values for the neighbors before computing the correlation. The simplest way to conceptualize Moran's I is to picture a slope of a plot, where the value of a focal point is plotted against the average value for its neighbors. When the values for the focal points are perfectly aligned with the neighbors, the slope is one; when the values for the focal point and its neighbors do not correspond to each other at all, the slope is zero. Formally, Moran's I is calculated by the following formula (using the example of calculating Moran's I for vegetation density across pixels in our AOI):

$$I = \frac{N}{W} \frac{\sum_{i=1}^{N} \sum_{j=1}^{N} w_{ij}(x_i - \bar{x})(x_j - \bar{x})}{\sum_{i=1}^{N}(x_i - \bar{x})^2}$$

The basic idea of the formula is to divide the covariance between neighboring pixels by the variance of pixel value in the whole image. The covariance in the formula is represented by the numerator, $\sum_{i=1}^{N} \sum_{j=1}^{N} w_{ij}(x_i - \bar{x})(x_j - \bar{x})$ divided by W. Here xi and xj are the vegetation density values at the focal pixel xi and neighboring pixel xj, x-bar is the average value of vegetation density in the AOI. Then the xi-x-bar is the departure from the mean for the focal pixel, and xj-xbar is the departure from the mean for the neighboring pixel. The product to the departures gives us the covariation between the pixels. The variable wij is a matrix of 0 and 1 values that determines which xi and xj pixels are considered neighbors. The sum of the values in the matrix is denoted as W. To calculate covariance from the covariations the covariations are averaged, in the formula they are summed together and divided by the number of values considered neighbors (i.e. the sum of "1" values in the wi,j matrix).

The variance in the formula is represented by the denominator, $\sum_{i=1}^{N}(x_i - \bar{x})^2$ divided by N. Here, N is the number of pixels in the image, and x is the vegetation density value for a given pixel in our dataset. The xi minus x-bar is the departure of the mean from any given pixel, which is then squared to eliminate negative values and calculate variation. The sum of the variations over all the pixels in the image divided by the total number of pixels gives us the population variance of the pixels.

For vegetation organized into patches, we would expect that points that are close in space will be highly autocorrelated and that this correlation will decrease over distance. However, data composed of periodic patterns show unique autocorrelation structure. The autocorrelation itself will become a periodic wave as the function is positively correlated when the neighbors are in phase, and negatively correlated when they are anti-phase. Therefore, to consider a pattern for the pattern as periodic, the ACF must oscillate between statistically significant positively and negatively correlated points. A full wavelength of the autocorrelation function corresponds to the dominant period in the vegetation data (Turchin 2003). To quantify these levels of correlation, we used Moran's I values. When the area of interest is entirely random, like the pixels of a broken television screen, Moran's I is approximately 0. A Moran's I value close to 1 would indicate very high levels of correlation, like when the tested function and neighbor are in phase.

Outputs

In our study, we used spatial autocorrelation analyses to characterize our area of interest by detecting significant spatial patterning, directionality, and periodicity of significant waves. To conduct our ACF analysis, we used the software PASSaGE 2 (PASSaGE 2 workflow included in the appendix). The first factor to consider when looking at the ACF results is the Moran's I value. If patterning is not present in the AOI, meaning that the data is completely spatially random, the ACF will be non-significant across all distances. On the other hand, if spatial patterning is present, the ACF function will have significant values. The shape of the ACF function, formed by the significant ACF values, helps determine the nature of the pattern. Specifically, graphs of autocorrelation (Moran's I over distance) inform us on what the spatial patterns of vegetation look like, such as if they are patchy or periodic. If the vegetation consists of patches that are not arranged periodically, the ACF would show a high Moran's I value or strong positive correlation, at short distances and the strength of the relationship would decrease towards zero at larger distances. Alternatively, when the vegetation patterns are organized in a periodic pattern, the ACF will oscillate between statistically significant positive and negative values (Figure 7).

Since we were seeking to examine the directionality of patterns in our AOI, we also noted whether the waves are isotropic or anisotropic. If the patterning is anisotropic, meaning the pattern only exists in one direction, the graph would differ significantly for varying directions. For example, an ACF for a simple cosine wave in space would show an oscillating ACF along the wave. However, if looking at the wave from a different direction it may have uniformly high correlation that does not oscillate across the wave. If it is isotropic, meaning the pattern exists in all directions, the graph will remain consistent for all directions we test for using ACF. Additionally, when interpreting the ACF it is important to be cognizant of the impact of the edges of our dataset. Since the edges of patches drive long distance autocorrelation, the analysis must use fewer neighbors, and therefore this results in lower resolution and lower reliability. To address this issue, we chose to limit our analysis to distances that were not impacted by edge effects.

We tested periodicity for both anisotropic and isotropic waves by looking at the presence of oscillations. In ACF, Moran's I values that decrease exponentially with distance, from values close to one to close to zero, suggest that the vegetation structure is patchy, but the patchiness is not oscillatory. In other words, if a graph of Moran's I over distance showed a decrease from one to close to zero over a short distance, the patterning is not periodic. Turchin (2003) states that ACF that oscillates between significant positive and negative values indicates periodicity (Figure 7). Turchin's recommendations were made, however, based on an insignificant amount of data. With significantly finer resolution and large datasets today, it is relatively easy to achieve statistical significance as results are less likely to reflect randomness. This presents a challenge for interpreting ACF functions that present seemingly random positive and negative statistically significant peaks. To address this issue, we implemented additional criteria before we classified an ACF as oscillatory: (1) the ACF had to show a minimum of three oscillations, and (2) the peaks and troughs in the ACF had to maintain a consistent spacing, signifying a consistent wavelength. We did not consider patterns to be periodic if they did not oscillate while holding constant amplitudes, wave lengths, and frequency.

If the ACF did not meet our criteria, the spatial organization may still be periodic, but over a larger scale than our study has accounted for. This points to the importance that scale has on the results of our study. Many factors impact the patterns at our field site, such as slope direction and steepness, that vary locally and so we expected that the periodicity of the patterns did not stay stable over larger areas. The hypothesis is that the pattern is locally periodic. This necessarily implies a question of at what scale are they stable enough to give a significant periodic signal. To address the question of scale, we subdivided the 100x100m AOI into 50x50m and 25x25m quadrants and performed the analyses separately at these scales.

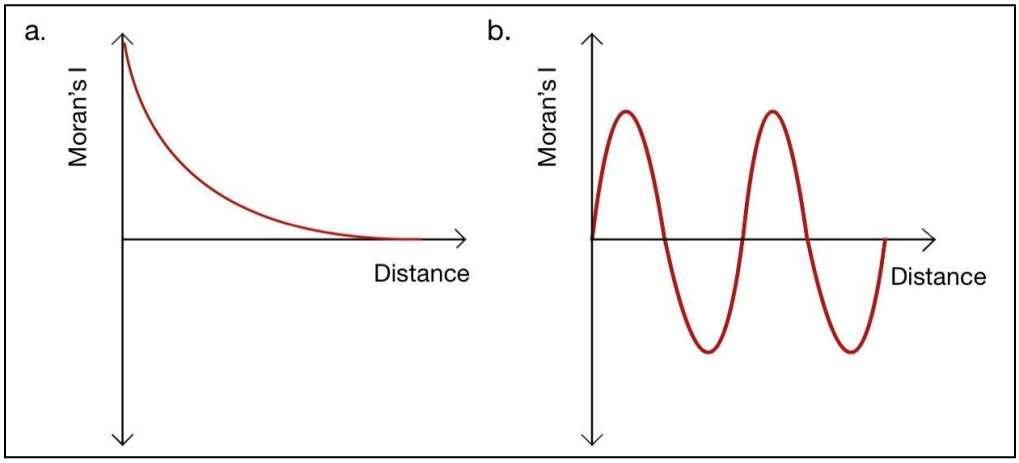

Figure 7: Example ACF graphs of spatial organization. Graph a. signifies that the landscape is patchy, has stationarity, but is non-periodic. Graph b. signifies that the landscape has periodic patchines

Results and Discussion

Analysis of Vegetation Patterning Over Time

In this study, we sought to determine if our AOI at Chico Basin Ranch shows periodicity when analyzed with Two-Dimensional Fast Fourier Transform (FFT) and the Autocorrelation Function (ACF) for the years 2019, 2017, 2005, and 2003. This question is of interest because it will improve understanding on the emergence of periodic vegetation patterns that plants develop as an adaptive strategy to increased aridity. As the climate in Colorado becomes increasingly arid, it is important to better understand the self-organization of desert vegetation and its periodic quality. This will better inform transitions in grassland ecosystems to desert, and to better conserve these regimes.

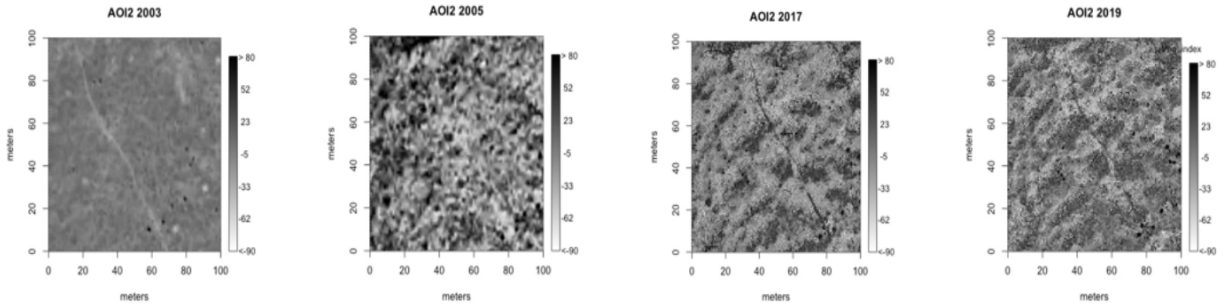

Figure 8. Aerial imagery of our AOI for years 2003, 2005, 2017, and 2019 in shades of gray

FFT and ACF Values

Table 9. Includes values of the 3 dominant wavelengths for the years 2019, 2017, 2005, and 2003. The dominant waves are highlighted to demonstrate the strength of analysis. Tables with a higher level of congruency, and therefore more highlighted values, show strong waves and potentially periodicity. Blue is used to indicate the three dominant waves for the year 2019 and the values are congruent with 2017 due to the similarity in their structure. Green represents the three dominant wavelength values for 2005, and yellow represents the three dominant wavelength values for 2003.

Table Key:

λ (m): wavelength in meters
Q: quadrant

Highlight Color Meaning

Blue: 3 Dominant Wavelength Values for 2019 and 2017
Green: 3 Dominant Wavelength Values for 2005
Yellow: 3 Dominant Wavelengths for 2003

Table 9.

2019	**FFT**			**ACF**		
	Wave 1	**Wave 2**	**Wave 3**	**Wave 1**	**Wave 2**	**Wave 3**
100x100m: λ (m)	15	19	16	105	105	105
Direction	116.5°	158°	71°	90°	120°	150°
Periodicity	Yes	Yes	Yes	Unclear	Unclear	Unclear
50x50m:Q1: λ (m)	14	14	22	15	15	15
Direction	°123	146°	153°	90°	120°	150°
Periodicity	No	No	No	Yes	Yes	Yes
Q2: λ (m)	14	14	22	19	19	19
Direction	123°	156°	153°	90°	120°	150°

Periodicity	No	No	No	Yes	Yes	Yes
Q3: λ (m)	25	16.2	36	22	22	30
Direction	90°	108°	135°	90°	60°	30°
Periodicity	No	No	No	Yes	Yes	Yes
Q4: λ (m)	26	16	7.2	-	-	-
Direction	135°	71.6°	135°	-	-	-
Periodicity	No	No	Yes	-	-	-
25x25: λ (m)	16.7	16.7	37	19	19	-
Direction	161°	108°	135°	0°	150°	-
Periodicity	No	No	No	Yes	Yes	No
Q2: λ (m)	12.5	10.4	-	12.5	12.5	12.5
Direction	135°	10°	-	120°	150°	0°
Periodicity	No	No	-	Yes	Yes	Yes
Q3: λ (m)	12.5	17	9	15	15	15
Direction	135°	108°	121°	90°	120°	150°
Periodicity	No	No	No	Yes	Yes	Yes
Q4: λ (m)	16.5	16.5	16.5	17	17	19
Direction	161°	°108	121°	90°	120°	150°
Periodicity	No	No	No	Yes	Yes	Yes

	2017	**FFT**			**ACF**		
		Wave 1	**Wave 2**	**Wave 3**	**Wave 1**	**Wave 2**	**Wave 3**
100x100m:	*λ (m)*	15	19	16	120	120	-
	Direction	116.5°	158°	71°	150°	120°	90°
	Periodicity	Yes	Yes	Yes	Yes	Yes	No
50x50m:Q1	*λ (m)*	14.2	18.7	8	15	15	15
	Direction	123°	158°	71°	90°	120°	150°
	Periodicity	No	Yes	Yes	Yes	Yes	Yes
Q2:	*Length(m)*	16	18	25	20	20	20
	Direction	108°	135°	90°	90°	120°	150°
	Periodicity	No	No	No	Yes	Yes	Yes
Q3:	*Length(m)*	25.5	16.6	23.8	22	22	22
	Direction	90°	108°	63°	90°	120°	60°
	Periodicity	No	No	No	Yes	Yes	No
Q4:	*Length(m)*	38.5	17	11.4	15	-	-
	Direction	135°	71°	116.5°	90°	-	-
	Periodicity	No	No	No	Yes	-	-
25x25:	*Length(m)*	10	-	-	20	20	20

	Direction	160°	-	-	120°	150°	0°
	Periodicity	No	-	-	Yes	Yes	Yes
Q2:	*Length(m)*	17.8	22.5	11.4	10	10	-
	Direction	45°	90°	26.5°	0°	30°	-
	Periodicity	No	No	No	Yes	Yes	-
Q3:	*Length(m)*	2	1.5	0.7	15	15	15
	Direction	135°	108°	145°	120°	150°	90°
	Periodicity	No	No	No	Yes	Yes	Yes
Q4:	*Length(m)*	17	17	17	18	-	-
	Direction	108°	161.5°	120°	120°	-	-
	Periodicity	No	No	No	Yes	-	-

	2005	**FFT**			**ACF**		
		Wave 1	**Wave 2**	**Wave 3**	**Wave 1**	**Wave 2**	**Wave 3**
100x100m:	*λ (m)*	105	24.4	105	62	62	62
	Direction	0°	104°	90°	0°	30°	60°
	Periodicity	No	Yes	No	Yes	Yes	Yes
50x50m:Q1:	*λ (m)*	51	51	25	-	-	-
	Direction	188°	0°	180°	-	-	-
	Periodicity	No	No	No	No	No	No
Q2:	*λ (m)*	17	24	51	23	23	19
	Direction	108°	90°	180°	°120	90°	150°
	Periodicity	No	No	No	Yes	Yes	Yes
Q3:	*λ (m)*	22.7	36	17	23	23	35
	Direction	63°	45°	72°	90°	120°	150°
	Periodicity	No	No	No	Yes	Yes	Yes
Q4:	*λ (m)*	36	23	12	-	-	-
	Direction	45°	63.4°	135°	-	-	-
	Periodicity	No	No	No	No	No	No
25x25:Q1:	*λ (m)*	37	37	7.35	-	-	-
	Direction	45°	45°	172°	-	-	-
	Periodicity	No	No	No	No	No	No
Q2:	*λ (m)*	37	37	10	25	27	-
	Direction	135°	135°	169°	0°	30°	-
	Periodicity	No	No	No	Yes	Yes	No
Q3:	*λ (m)*	6	16.6	12.3	7	7	17
	Direction	144°	108°	135°	120°	150°	60°
	Periodicity	Yes	No	No	Yes	Yes	Yes

Q4:	*λ (m)*	-	-	-	23	23	-
	Direction	-	-	-	30°	60°	-
	Periodicity	-	-	-	Yes	Yes	No

	2003	**FFT**			**ACF**		
		Wave 1	**Wave 2**	**Wave 3**	**Wave 1**	**Wave 2**	**Wave 3**
100x100m:	*λ (m)*	45	71.4	45	35	35	-
	Direction	26.6°	45°	116.6°	90°	60°	-
	Periodicity	No	No	No	Yes	Yes	No
50x50m:Q1:	*λ (m)*	51	51	22.7	40	40	50
	Direction	180°	0°	153°	90°	120°	150°
	Periodicity	No	No	No	Yes	Yes	Yes
Q2:	*λ (m)*	51	35.7	17	50	50	50
	Direction	90°	135°	0°	90°	120°	150°
	Periodicity	No	No	No	Yes	Yes	Yes
Q3:	*λ (m)*	14	36	23	-	-	-
	Direction	34°	45°	116.6°	-	-	-
	Periodicity	No	No	No	-	-	-
Q4:	*λ (m)*	35.7	51	22.7	-	-	-
	Direction	45°	90°	26.5°	-	-	-
	Periodicity	No	No	No	-	-	-
25x25:Q1:	*λ (m)*	16.7	37.3	37.3	-	-	-
	Direction	108.4°	45°	45°	-	-	-
	Periodicity	No	No	No	No	No	No
Q2:	*λ (m)*	37.3	-	-	-	-	-
	Direction	135°	-	-	-	-	-
	Periodicity	No	-	-	No	No	No
Q3:	*λ (m)*	17	10.2	7.35	23	-	-
	Direction	72°	101°	9°	90°	-	-
	Periodicity	No	No	No	Yes	No	No
Q4:	*λ (m)*	16.5	16.5	12.3	23		
	Direction	161°	162°	45°	0°	-	-
	Periodicity	No	No	No	Yes	No	No

2019

Visual inspection of the image of our AOI of Chico Basin Ranch from 2019 showed vegetative patterning in the landscape. There appear to be periodic patches of vegetation bisected with sections of bare ground. They are visually evenly spaced in the NW-SE direction. FFT extracted the three dominant wavelengths underlying this pattern. At the 100 by 100-meter scale, dominant wavelengths of 15 meters, 19 meters, and 16 meters lie in the NW-SE direction (116.5 degrees, 158 degrees) and NNE-SSW (71 degrees). Each wave repeated itself over 5 times across the area of interest and therefore by our criteria, indicated that the pattern was periodic.

FFT at smaller scales, including 50x50 and 25x25 meter quadrants, consistently displayed a NW-SE orientation of the waves which is congruent with the 100x100 meter quadrant FFT. All but one of the dominant wavelengths occur in the general NW-SE direction, though the precision of the direction becomes less exact with the angles of direction varying up to 20 degrees between quadrants. In contrast to the 100x100m FFT, the FFT for 50x50 and 25x25 meter quadrants have much lower wavenumbers across the AOI for the three dominant wavelengths. Because fewer of the waves meet the conventional requirement of a minimum of four full oscillations to be considered periodic, this means that FFT detected periodicity less often at the 50x50 and 25x25m scales. Given the decrease in detected periodicity, we can conclude that these quadrants are the wrong scale to detect periodic patterns. They are too small, preventing the waves from oscillating four or more times over the quadrants. Therefore, 100x100 meters is a more accurate scale than 50x50 or 25x25 meter quadrants for analyzing desert vegetation patterns at Chico Basin Ranch using FFT.

This is not the case for our ability to detect periodic patterns using the autocorrelation function (ACF). ACF at the 100x100 meter scale shows waves moving in the NW-SE direction (90, 120, and 150 degrees), congruent with the 100x100 meter FFT. However, the wavelengths detected by ACF are approximately 105 meters long, which is incongruent with FFT. The wavelengths given by ACF at this scale are the same length of the quadrant, which means it only oscillates once. This wave number is too small to determine whether the pattern is periodic. Therefore, the conclusion from the 100x100m ACF is that the vegetation is patchy but not periodic and that the patchiness is anisotropic. Scaling down to 50x50 and 25x25 meter quadrants displayed significant periodicity that was congruent results when compared to the 100-meter FFT. A majority of the detected waves had strong levels of congruency with the 100x100m FFT, consistently moving in the NW-SE direction with wavelengths of 10 to 20 meters.

However, one of the waves in quadrant four for both the 25x25 and 50x50 meter ACF oscillated only once in the AOI, which does not qualify the pattern as periodic. The lack of periodicity in quadrant 4 is an outlier among the other quadrants, which all have excellent periodicity in the NW-SE direction with most of the wavelengths in the range of 10 to 20 meters. This suggests that a majority of the AOI displays periodic patterning, with a small corner that does not display patterning congruent to the rest of the quadrant. The ACF analysis at the 25x25 and 50x50 meter scale clearly showed oscillating patterns and it appears that the 25x25 and 50x50 meter scale is appropriate for detecting periodic patterns in our system using ACF.

Based on our analysis of the 2019 AOI, there appears to be periodic patterning in vegetation. The congruence between 100x100 meter FFT and 25x25 and 50x50 meter ACF between quadrants points to the periodicity of the dominant wavelengths of 15 to 20 meters and the anisotropic quality of the pattern in the NW-SE direction.

2017

Our analysis clearly detected periodicity in vegetation structure three years prior, in 2017. From the qualitative visual analysis of the image, the landscape appears to be spatially organized in a periodic striped pattern. Much like in 2019, there are clear directional patterns evenly alternating between vegetation and bare ground, moving Northwest-Southeast. Once again, this analysis is backed up by a 100x100 meter FFT analysis. The periodogram generated by FFT at 100x100 meters shows the waves one and two moving in the NW-SE direction and wave three moving NNE-SSW with all three dominant wavelengths of 15-20 meters. The wave numbers are all greater than 5, signifying the periodicity of the dominant waves. When looking at the FFT results from the 50x50 and 25x25 meter quadrants, it is clear the results show congruency in wave direction. However, the scale is too small to correctly detect periodicity in the dominant wavelengths present. The wave numbers decreased to below three, which is shown by the waves inability to oscillate enough times to consider them periodic over the shortened distance of the now smaller quadrants.

As in the 2019 analysis, the 100x100 meter ACF showed a wave direction that was congruent to the 100x100 meter FFT. However, the associated wavelengths and wave numbers were again on the same spatial scale as the AOI, making it difficult to conclude the pattern was periodic. ACF at smaller scales of 25x25 and 50x50 meter quadrants is better suited at detecting periodicity for our AOI. The 50x50 meter ACFT has strong congruence with 100x100 meter FFT and even 50x50 meter FFT, with NW-SE direction (120° and 150°) as the most common orientation for periodic waves, with wavelengths of 15 to 20 meters. The 25x25 meter ACF analysis shows congruence in the NW-SE direction and in wavelength. However, because the wavelengths are a similar size to the length of the quadrant, it is difficult to detect periodicity at the 25x25m scale.

Congruence between different methods of analysis for direction, wavelength, and periodicity within the same year speaks to the strength of the patterning present. Additionally, it is important to note congruences between different years to understand the persistence of such patterning. In the case of 2017, there is not only congruence between the methods of analysis within the, but there is also congruence in direction, length, and periodicity with the 2019 data and analysis. This shows that the periodic patterning in the NW-SE is persistent and significant throughout the ecological regime of this area of Chico Basin Ranch during the period of 2017-2019.

2005

Analysis from over 10 years beforehand tells a different story. The visual inspection of the aerial image from 2005 shows distinct vegetation patches. However, these patches visually appear to have no clear organization as they are unevenly distributed throughout the AOI. Both our FFT and ACF methods

of analysis reflect this lack of organization. The 100x100 meter FFT shows three dominant wavelengths of 105 meters, 24.4 meters, and 90 meters oriented in a NE-SW direction (0°, 104°, and 90°). The wave numbers ranged from one to four, meaning that we can only consider one of the dominant waves borderline periodic due to its wave number of four.

When scaling the analysis to 50x50 and 25x25 meter quadrants, FFT was unable to detect periodicity for our AOI. This may be because there is none, though we can also argue that it is because the scale of the AOI is not appropriate for detecting 24m long waves since it is too small to allow four or more replications of the wave. FFT analysis at the 50x50 and 25x25m scale also shows incongruence in direction and inconsistent wavelengths among the quadrants. The orientation of waves varies between quadrants, indicating that there isn't one consistent pattern throughout the AOI.

ACF analysis is similar to the FFT analysis in that it has major inconsistencies between quadrants of the same scale. Additionally, these inconsistencies do not align with the FFT results for the same quadrants. In the 100x100 meter quadrant, the dominant directions of NE-SW (0°, 30°, and 60°), with a dominant wavelength of 61 meters, is different from the 100x100 meter FFT both in direction and wavelengths. The wave directions shifted on the 50x50 meter scale to ESE-WNW (90°and 120°), and on the 25x25 meter scale to SE-NW (120° and 150°) and ENE-SWS (30° and 90°). ACF analysis detected that these directions have periodic wavelengths, and between quadrants of the same sized scale there is some congruence. This indicates that small areas may have detectable periodic patterns, though the patterns switch directions and wavelengths.

2003

The FFT and ACF analysis of periodic spatial patterns for 2003 is similar to that of 2005. The image is visually slightly patchy with no distinct organization. Some areas appear lighter, meaning they are less vegetated, while others are notably darker, meaning they are more vegetated. However, it is hard to distinguish between individual patches throughout the AOI. The 100x100 meter FFT analysis, as expected given the image, does not show any periodicity. The three dominant waves detected are oriented in the NE-SW direction (26.6°, 45°, and 116.6°), which is congruent to some of the 2005 data analysis, with wavelengths ranging from 45 meters to 71.4 meters.

There is little congruence detected, however, by any of the proceeding analysis of smaller scaled FFT or ACF. On the 50x50 meter scale for ACF, there is some directional congruence within quadrants, with wave directions falling within the ESE-WSW (90° and 150°) range. There is also some periodicity detected, with wavelengths of 50 meters. However, it is unlikely this periodicity is accurate given they are the same size as our AOI quarters and can therefore only complete one repetition. This, as well as incongruence with the 100x100 meter FFT, leads us to believe there is not periodicity in 2003 at this area of Chico Basin Ranch.

The 25x25 meter FFT and ACF analysis, which are neither congruent between quadrants nor each other, further confirmed this conclusion. Different patterns shown by different methods of analysis shows that there are no dominant periodic waves in this regime. Therefore, the lack of congruency in

2003 and 2005 show us that there is no periodic patterning at Chico Basin in this period of time. Any patterning present is inconsistent in direction and is limited to small portions of the area of interest, showing non-stationarity. Additionally, this data shows no congruency in vegetative patterning to that of 2017-2019, suggesting that a regime shift in this area of Chico Basin Ranch must have occurred in the intermediary period for the emergence of periodic vegetative patterns to occur.

Intent of Study

Our study aims to answer a two-part question about the spatial organizational patterns of arid grassland vegetation, specifically the distribution of blue grama in Chico Basin Ranch, CO. The first part of our question begins with determining how to use statistics in order to identify patterns present in the system with confidence. There is no clear consensus in the literature of how outputs should be analyzed to determine the confidence of results, so it was crucial that our study determine the outputs at which we are confident periodic patterns exist in our vegetation structure. Our second question seeks to examine if there is a change in vegetation structure from non-patterned to patterned over time. There have been many theoretical studies that consider the shift from a non-patterned homogenous state to a patterned state predicts a catastrophic change of stable states to desertification. Therefore, it is important to determine if this shift is occurring at Chico Basin Ranch as a warning sign before more catastrophic changes occur.

We chose to use two methods of analysis for our study, 2D Fast Fourier Transform and ACF. The main reason for using both methods was that each has its own set of shortcomings when used in isolation. FFT is applied to a specific window of the area of interest, which can cause scale-based challenges. If waves do not fit within the window, FFT has a tendency of truncating the wave thus providing an inaccurate wavelength and wave number (Ford and Renshaw, 1984). We can remedy this concern in part by adjusting the window size and location, as well as determining which wavenumbers occur below the threshold of periodicity. FFT may identify non-periodic patchiness at scales similar to the area of study as statistically significant for low frequency waves (Ford and Renshaw, 1984). To overcome this concern in our study, we determined that the waves must have a threshold wavenumber of four to consider them as periodic. However, this is not a perfect method (Penny, 2013).

Therefore, ACF is a useful tool to use in conjunction with FFT. Congruence between results ensures accuracy because ACF can indicate periodicity very clearly. When the dataset is periodic, the Moran's I value will alternate between significant positive and significant negative values, creating its own periodic wave (Turchin, 2003). In contrast, if the dataset represents a landscape that is patchy but not periodic, the graph of Moran's I values over distance will show high Moran's I values initially that decrease to zero and level out at zero as distance increases. Therefore, ACF can indicate when a wave is patchy but not periodic, where FFT might truncate the wave and indicate periodicity where it is not present. ACF, however, is not without shortcomings. While ACF identifies the dominant wave period, it is unable to identify the individual simple waves (Turchin, 2003) . This is why it is valuable to use ACF in conjunction with FFT. The ideal combination that accounts for the concerns with each method is to use ACF first to determine that periodicity exists, and then follow up with an FFT analysis to further determine the unique details of the simple waves. However, our analysis shows that finding congruency

between FFT and ACF may be more complicated than expected because the two methods have different levels of sensitivity when detecting waves. In our analysis, congruence came at different scales with ACF at 50 by 50 meters showing congruent results to FFT, but at the 100 by 100 meter scale. FFT appears to need a larger AOI to detect periodicity when we consider the threshold of periodicity to be four waves, whereas ACF is not sensitive enough to detect waves at that scale.

Through our 2D FFT and ACF analysis, we were able to identify the presence of dominant wavelengths for the years 2019 and 2017. For 2019, which has visually distinct patterns, the FFT and ACF analysis had congruent results of wavelengths arranged broadly perpendicular to hill slope. The waves range from 15 to 20 m and wave directions in the NW-SE direction at 100x100-50x50m. This means that there is significant periodic patterning for this system during 2019. Similarly, the results from FFT and ACF for the year 2017 are congruent and show that the vegetation has significant periodicity. Additionally, the wave lengths and directions are nearly identical to our 2019 results and have congruently high levels of stability. In contrast, the years 2005 and 2003 FFT and ACF analysis show incongruent results that we interpreted as signifying patchy vegetation with no significant periodic patterning over the 100x100m or 50x50m scale. An alternate conclusion is that for the years 2003 and 2005, there may be periodic patterning present but at different scales than the analysis considered.

Ecological Significance

These results signify that patterning of blue grama grass emerged between the 2003-2005 period and the 2017-2019 period. The increase in patterning over this time period is consistent with the significant decrease in vegetation cover found by a study on the change in species composition and climatic conditions at the Chemical Depot (Rondeau, 2016), which is a similar environment to Chico Basin ranch and located 30 km south of our field site. The study in comparison, conducted by the Colorado Natural Heritage Program from CSU Fort Collins, CO., took place from the years 1998-2015. They found a 50% decrease in blue grama density, defined as the number of plants over an area, from 1998 to 2015. These results are congruent with the results of our study, as a decrease in blue grama density before the years 2017 and 2019 is consistent with the increase in bare ground that make up periodic vegetation patterning that FFT and ACF identified for our study site. At Chico Basin Ranch, the decrease in blue grama density did not occur homogeneously throughout the landscape, but in periodic bands that now appear as bare ground. Since the periodic vegetation patterns in our study site are made up of stripes of blue grama grass alternating with stripes of bare ground, the density of blue grama grass has decreased with the presence of bare ground bands.

While the formation of patterns appears to be directly related to a decrease in blue grama density, it is important to understand how change in precipitation may also contribute to the spatial organization of blue grama. Rondeau (2016) correlated the decrease in blue grama density with extreme drought years, occurring in 2002 and the period from 2010-2012. The response of the blue grama to drought conditions was not immediate and experienced a lag of at least a year before they measured a decrease in vegetation density. The same regional drought may be driving the changes in the vegetation patterning at our field site. Additionally, the large decline in vegetation density persisted despite higher levels of precipitation in 2014 and 2015. This indicates that a few years of adequate rainfall may not

reverse the results of years of drought conditions (Rondeau, 2016). The mechanics that drive the feedback of drought-induced periodic spatial organization include short range facilitation, in which patches of grass collect water from runoff from above slope, and long-range inhibition where the water retention of patches limits the amount of water available to other plants below their patches.

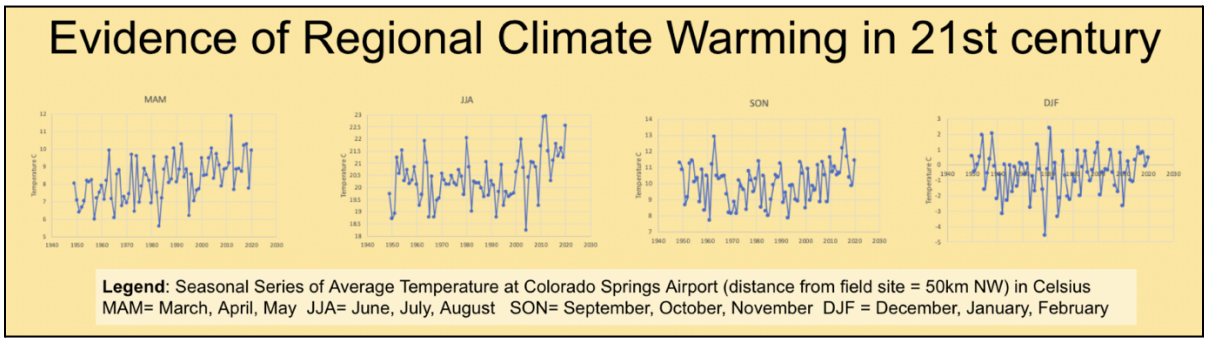

Figure 8. Graphs showing climate warming 27 km south from Chico Basin Ranch (McDonald et al. 2021)

Additionally, overall regional warming has been increasing steadily throughout the 21st century, which may increase evaporative stress for blue grama grass (McDonald et al., 2021). These conditions will further promote changes in vegetation patterning, as patterning will allow plants to maintain a portion of their population despite more challenging conditions. However, the increased patterning results in decreased resilience of the blue grama population (Mayor, 2013). One way in which blue grama resilience will decrease is that their striped patches will move up slope. As runoff of water decreases, the run-on system will not reach the lower portion of the stripes. Receiving water only from precipitation, which is decreasing in quantity, will not be sufficient to support the lower portion of the grove (Rietkerk, 2008). Therefore, the lower portion of the stripes will die, and the remaining vegetation will move upwards towards the direction of more water flow (Dunkerly, 2018). Additionally, decreasing the size of patches will reduce resilience as increasing stripes of bare ground will limit the short-range facilitative processes. The size of vegetation patches will have to shrink because the amount of water that short-range facilitation acquires will no longer support the full population. The decreased ability of the blue grama to facilitate their populations will minimize their resistance to worsening drought conditions (Mayor, 2013).

Conservation Implications

Since spatial patterning is a strong indicator for reduced resilience leading to a potential state change from vegetated to desert conditions, monitoring the development of patterns is important for conserving ecosystems. At Chico Basin Ranch, monitoring efforts are currently limited to small plots distributed over the extent of the ranch. While this is a strong start, small quadrants are unable to capture changes in spatial organization over the scale at which this patterning is occurring. The small scale of monitoring is likely leading to an inaccurate understanding of the current state of this ecosystem and how it may be changing. We recommend that monitoring efforts should instead occur at a larger scale, using aerial imagery to capture bigger AOIs. Increasing the scale of vegetation monitoring will

show a more accurate picture of ecosystem health by including large scale pattern formation. Our study shows that the formation of periodic patterning emerged in the years between 2003-2005 and 2017-2019. Monitoring the development of spatial patterning to see if it persists will be valuable to determine the resilience of the blue grama. This is a crucial first step in understanding if the stewards of this landscape need to take action to mitigate the issue. This study did not examine potential mitigation efforts, though an example include adjusting the timing and stock density of grazing practices in order to prevent desertification.

Work Cited

Dunkerley, D. (2018). Banded vegetation in some Australian semi-arid landscapes: 20 years of field observations to support the development and evaluation of numerical models of vegetation pattern evolution. Desert, 23(2), 165-187.

Ford, E. D., & Renshaw, E. (1984). The interpretation of process from pattern using two-dimensional spectral analysis: modeling single species patterns in vegetation. Vegetation, 56(2), 113-123.

Foster, E. (2021). Identifying Variations within the Runoff-Runon System of Self-Organizing Arid Vegetation.

Ludwig, J.A., Tongway, D.J., Marsden, S.G., 1998. Stripes, strands or stipples: Modeling the influences of three landscape banding patterns on resource capture and productivity in semi-arid woodlands, Australia. Catena, this issue.

Malanson, George P., et al. (2011). "Mountain treelines: a roadmap for research orientation." Arctic, Antarctic, and Alpine Research, 43.2, 167-177

Mayor, A. G., Kéfi, S., Bautista, S., Rodríguez, F., Cartení, F., & Rietkerk, M. (2013). Feedbacks between vegetation pattern and resource loss dramatically decrease ecosystem resilience and restoration potential in a simple dryland model. Landscape ecology, 28(5), 931-942.

McDonald, A., Foster,E., Jennings, A., McMullin, E., Buchband, H., Kummel, M. (2021). Desertification in arid Colorado shortgrass steppe? Emerging periodic vegetation pattern formation, possibly driven by climate change, ESA Conference

Noy-Meir, I. (1973). Desert Ecosystems: environment and producers. Annu. Rev. Ecol. Systematics 4, 25-51

Penny, G. G., Daniels, K. E., & Thompson, S. E. (2013). Local properties of patterned vegetation: quantifying endogenous and exogenous effects. Philosophical Transactions of the Royal Society A: Mathematical, Physical and Engineering Sciences, 371(2004), 20120359.

Renshaw, E., & Ford, E. D. (1983). The interpretation of process from pattern using two-dimensional spectral analysis: methods and problems of interpretation. Journal of the Royal Statistical Society: Series C (Applied Statistics), 32(1), 51-63.

Renshaw, E. and Ford, E.D. (1984). The Description of Spatial Pattern Using Two-Dimensional Spectral Analysis, Vegetation, 56:75-85

Rietkerk, M., SC. Dekker, SC., de Ruiter, PC., van de Koppel, J. (2004). Self-organized patchiness and catastrophic shifts in ecosystems. Science, 305; 1926-1929. DOI: 10.1126/science.1101867.

Rietkerk, M., & Van de Koppel, J. (2008). Regular pattern formation in real ecosystems. Trends in ecology & evolution, 23(3), 169-175.

Rondeau, R.J., G.A. Doyle, and K. Decker. 2016. : 1999-2015. Colorado Natural Heritage Program, Colorado State University, Fort Collins, Colorado.

Scheffer, M., Carpenter, S., Foley, J. A., Folke, C., & Walker, B. (2001). Catastrophic shifts in ecosystems. Nature, 413(6856), 591-596.

Scheffer, M., & Carpenter, S. R. (2003). Catastrophic regime shifts in ecosystems: linking theory to observation. Trends in ecology & evolution, 18(12), 648-656.

Turing, A. M. (1990). The chemical basis of morphogenesis. Bulletin of mathematical biology, 52(1), 153-197.

Vandervaere, J. P., Peugeot, C., Vauclin, M., Jaramillo, R. A., & Lebel, T. (1997). Estimating hydraulic conductivity of crusted soils using disc infiltrometers and minitensiometers. Journal of Hydrology, 188, 203-223.

Appendix

PASSaGE 2 steps

Step 1: Data input

To upload data, we clicked the top left icon on the Passage interface. This allowed us to upload a file from the computer, making sure it is comma delineated. Then, we selected a rectangular matrix and the "contains column headings'' feature. We repeat this step with the same data set for "coordinates," select "contains column headings," and select 2 columns, x and y.

Step 2: Making Distance and Angle Coordinates

Under create, we then select the icon for Distances/Angles for Coordinates, ensuring both the distance and angle boxes are selected.

Step 3: Distance Classes

Under create, we selected distance classes. For "Each class with equal observation," we set classes to 20 and the number of observations to 2499750. For "each class of equal width," set classes to 10 and left the width of observations as is.

Step 4: Correlograms

For the first correlogram, we selected the correlogram icon in Analysis 2. Then, we deselected x and y and selected the CI feature, making sure that the "Save output to Matrix" was saved before moving on.

For the second correlogram, we selected the Anisotropy icon and then "Bearing Correlogram in the drop down. Again, we deselect x and y and ensure that the "Save output to Matrix" is saved.

2D FFT Code, Co-written by Miro Kummel and Amelia McDonald

############################## 2D spectral analysis of raster data##############################

#This code outputs the 2D periodogram, angular spectrum, radial spectrum and resampled confidence band for the
#angular and radial spectra based on complete spatial randomness

###3.3.2021
Code author: Miro Kummel in collaboration with Amelia McDonald

basis for the code: Ford and Renchaw, matlabcode supplied by Johan Vandecolle

##

#Connecting R to a folder that the images are in and that will receive any saved output from the analysis

```
#setwd("C:/Users/Miroslab/Desktop/Chico_periodicity")
#getwd()
setwd("/Users/mkummel/Desktop/Waves_and_Fourier")
getwd()

#activating libraries of packages that are necessary to do the FFT (spectral) and to handle the images
library(spectral)
library(raster)
library(rgdal)

# Acquiring the image
###THE IMAGE MUST BE MONOCHROMATIC####
AOI.tiff <- raster("AOI2_Bsq05m.tif")
AOI.tiff #gives you basic information about the tiff
plot(AOI.tiff) #plots the tiff

#extracting the matrix that codes the image
mat.AOI.tiff<- as.matrix(AOI.tiff) #isolated matrix, got rid of extra stuff like the geospatial info

#########EXTREMELY IMPORTANT!!!!!#########
dim(mat.AOI.tiff) # this step is to check that the matrix is square and has even number of rows and
columns
#!!!!!!THE MATRIX MUST BE SQUARED AND MADE EVEN NUMBERED!!!!!
#if it is not square i.e. row number != column number e.g. 181x180
# or if it has odd number of rows ..e.g. 201x201 it has to be fixed here
#for example if mat.AOI.fiff is 181x180 the following code will square it and make it even
#mat.AOI.tiff<-mat.AOI.tiff[1:180,1:180]

#rotating the matrix so when plotted North in north
rotate <- function(x) t(apply(x, 2, rev))
AOI<-rotate(mat.AOI.tiff)

#this sets out the x and y coordinates for the image and the analysis
x <- seq(0, 1, length.out = dim(AOI)[1])
length(x) #must be the same as number of rows in the image matrix
y <- seq(0, 1, length.out = dim(AOI)[2])
length(y) #must be the same as number of columns in the image matrix

#centering the values of the image matrix to fluctuate around zero
#by subtracting the mean value of the image matrix from the mean
mean.AOI <- mean(AOI) #calculate mean
m<-AOI-mean.AOI
min(m)#must be a negative number
```

```
#plotting the adjusted image
#... the overall impression has to be the same as the original,
rasterImage2(x = x,
        y = y,
        z = m,
        main = "image matrix")

########## calculate the spectrum###############
FT <- spec.fft(x = x, y = y, z =m)
# initially plotting the full spectrogram ... this is so we know what part to focus on
plot(FT)
#in this particular example we should focus on -30 to 30 for both x and y axes
plot(FT, xlim=c(-30,30), ylim=c(-30,30))
#checking that the output of FT looks good
#should include two vectors of real numbers and a matrix of complex numbers
FT

#Extracting components of the FT output
fx<-FT$fx
fy<-FT$fy
I<-abs(FT$A)

#plotting the image of matrix I as a mid-processing check
#if the plot looks the same as the previous plot of FT, then this is successful
#please adjust the xlim and ylim as in line 73
rasterImage2(x = fx,
        y = fy,
        z = I,
        xlim = c(-30, 30),
        ylim = c(-30, 30),
        main = "matrix I")

#calculating variance of the image as represented by matrix m
mean.m <- mean(m) #calculate mean
m.prime <- m-mean.m #calculating departures from the mean
m.prime.squared <- m.prime^2 #calculating "squares"
sum.squares <- sum(m.prime.squared) #add squares together to get sum of squares
variance.m <- sum.squares/(dim(m)[1]*dim(m)[2]) #divide by sample size

##################################FINAL PERIODOGRAM#####################################
#preparing the variogram that actually gets analyzed
I.2<-I^2
```

```
I.mr <- (dim(m)[1]*dim(m)[2])*I.2
I.final <- I.mr/variance.m
#export out the I.final --- please make sure you save it with a recognizable name
write.csv(I.final, file="I.final.AOI2_bigsq.csv")
#Plotting the periodogram that will be basis of the final analysis
#please do not forget to adjust the xlim and ylim as in the lines 89 and 90
#please export this image as PDF
rasterImage2(x = fx,
        y = fy,
        z = I.final,
        xlim = c(-30, 30),
        ylim = c(-30, 30),
        main = "AOI 2")

###################################ANGULAR SPECTRUM#####################################

#Extracting the "top half" of the periodogram
I.for.analysis<-I.final[,(1+.5*length(fy)):length(fy)]
dim(I.for.analysis)
#adjusting the vector that dictates the y axis to correspond to the halved periodogram
fy.for.analysis<-fy[(1+.5*length(fy)):length(fy)]

#####THETA Matrix is a matrix of angles################
#used to divide the periodogram into vedges
theta.matrix<-matrix(NA,nrow=length(fx),ncol=length(fy.for.analysis)) #same dimension as I.for.analysis
#check that the theta matrix has the same dimensions as I.for.analysis
dim(theta.matrix)
#calculating angles .... zero is pointing east
for (i in 1:length(fx)){
  for (j in 1:length(fy.for.analysis)){
    theta.matrix[i, j] <- (180/pi)*atan2(fy.for.analysis[j],fx[i])
  }}
#mid-processing check --- this should look like a fan
image(theta.matrix)

###############setting up the parameters for angular spectrum#########
##the parameter to adjust here is the bin size.
#10 degrees is a good start, but I had better luck with 5
ang.bin.size<-5 # if you divide 180 by this number you get the number of bins
ang.bin.number<-180/ang.bin.size #needs to be an integer
ang.bin.cutoffs<-seq(from=0,to=180,by=ang.bin.size)
ang.bin.cell.counter<-numeric(length = ang.bin.number) #counts number of pixels
ang.bin.aggregated.signal<-numeric(length = ang.bin.number) #sum of values of all pixels counted above
```

```
#ang.bins are the centers of the ang bin cut offs for plotting
ang.bins<-(ang.bin.cutoffs[1:(length(ang.bin.cutoffs)-1)]+ang.bin.cutoffs[2:(length(ang.bin.cutoffs))])/2

####This loop does the angular spectral analysis############
for (a in 1:ang.bin.number){ #180/10
  for (i in 1:length(fx)){ #length of x-axis
    for (j in 1: length(fy.for.analysis)){ #length of y-axis
      if(theta.matrix[i,j]>=ang.bin.cutoffs[a]&theta.matrix[i,j]<ang.bin.cutoffs[a+1]){
        ang.bin.cell.counter[a]<-ang.bin.cell.counter[a]+1
        ang.bin.aggregated.signal[a]<-ang.bin.aggregated.signal[a]+I.for.analysis[i,j]
        }}}}

#Plotting the angular spectrum as a mid-processing check
ang.bin.averaged.signal<-ang.bin.aggregated.signal/ang.bin.cell.counter
plot(ang.bins,ang.bin.averaged.signal,type="l")#mid-processing check

############################RADIAL SPECTRUM ANALYSIS ###################################
#setting up the radial matrix
radial.matrix<-matrix(data=0,nrow=length(fx), ncol=length(fy))
#populating the radial matrix with distances from the (0,0) on fx and fy vectors
for (i in 1:length(fx)){
  for (j in 1:length(fy)){
    radial.matrix[i, j] <- ((fx[i]^2)+(fy[j])^2)^0.5 #calculates data of pixels from each direction ie distance
from center
  }}
#mid processing check on the radial matrix --- should look like tree rings
image(radial.matrix) #mid-processing check

#########Setting up parameters for the radial spectrum
r.max.mk<-70 #has to be a whole number, look for the largest value in the radial matrix and round down
r.bin.size<-0.5 #THIS IS WHERE BIN SIZES ARE ADJUSTED ... 1 is also a good number
r.bin.number<-r.max.mk/r.bin.size
r.bin.cutoffs<-seq(from=0,to=r.max.mk,by=r.bin.size)
r.bin.cell.counter<-numeric(length = r.bin.number) #counts number pixels per bin (as we move out, the
number of pixels increases)
r.bin.aggregated.signal<-numeric(length = r.bin.number) #sum on values of pixels
r.bins<-(r.bin.cutoffs[1:(length(r.bin.cutoffs)-1)]+r.bin.cutoffs[2:(length(r.bin.cutoffs))])/2

####this loop does the radial analysis#################
for (a in 1:r.bin.number){
  for (i in 1:length(fx)){
    for (j in 1: length(fy)){
      if(radial.matrix[i,j]>=r.bin.cutoffs[a]&radial.matrix[i,j]<r.bin.cutoffs[a+1]){
```

```
      r.bin.cell.counter[a]<-r.bin.cell.counter[a]+1
      r.bin.aggregated.signal[a]<-r.bin.aggregated.signal[a]+I.final[i,j]
      }}}}

##########plotting the results of the radial analysis as a mid-processing check
r.bin.averaged.signal<-r.bin.aggregated.signal/r.bin.cell.counter
plot(r.bins,r.bin.averaged.signal,type="l")#mid-processing check

#############################################################################
### Resampling to determine statstical significance in comparison to CSR#######
#############################################################################
#here we adjust the number of time we scramble the matrix --- the number of bootstraps
num.scrambles<-100
# This sets up matrices to record the results of the bootstrapping
#angular spectrum results matrices
ang.bin.cell.counter.scramble<-matrix(data=0,nrow = ang.bin.number,ncol=num.scrambles) #counts
number of pixels
ang.bin.aggregated.signal.scramble<-matrix(data=0,nrow = ang.bin.number,ncol=num.scrambles) #sum
of values of all pixels counted above
#radial spectrum results matrices
r.bin.cell.counter.scramble<-matrix(data=0, nrow = r.bin.number, ncol=num.scrambles) #counts number
pixels per bin (as we move out, the number of pixels increases)
r.bin.aggregated.signal.scramble<-matrix(data=0, nrow = r.bin.number, ncol=num.scrambles) #sum on
values of pixels

###########THis code does the resampling###################
#WARNING: depending on the number of scrambles it may take several minutes of hours to rum
dim.m<-dim(m)
for (s in 1:num.scrambles){
m.resam<- matrix(0, nrow=length(x), ncol=length(y))
for (i in 1:dim.m[1]){
  for (j in 1:dim.m[2]){
    x.cord<-sample(1:dim.m[1], size=1, replace=TRUE)
    y.cord<-sample(1:dim.m[2], size=1, replace=TRUE)
    m.resam[i,j]<-m[x.cord, y.cord]
  }}

# calculate the spectrum
FT <- spec.fft(x = x, y = y, z = m.resam)
#############################################################################
I<-abs(FT$A)
#############################################################################
```

```
#figuring out how to relate variance of the data to the periodogram
#step 1: calculate variance of matrix (m)
mean.m.resam <- mean(m.resam) #calculate mean
m.resam.prime <- m.resam-mean.m.resam #calculating departures from the mean
m.resam.prime.squared <- m.resam.prime^2 #gets rid of negatives and shows stronger values
sum.squares <- sum(m.resam.prime.squared) #add squares together
variance.m.resam <- sum.squares/(dim(m.resam)[1]*dim(m.resam)[2]) #divide by sample size
variance.m.resam
I.mr <- (dim(m.resam)[1]*dim(m.resam)[2])*I^2
I.final <- I.mr/variance.m.resam
##############################################################################

#calculating the theta matrix
fx<-FT$fx
fy<-FT$fy

I.for.analysis<-I.final[,(1+.5*length(fy)):length(fy)]
fy.for.analysis<-fy[(1+.5*length(fy)):length(fy)]

for (a in 1:ang.bin.number){ #180/10
  for (i in 1:length(fx)){ #length of x-axis
    for (j in 1: length(fy.for.analysis)){ #length of y-axis
      if(theta.matrix[i,j]>=ang.bin.cutoffs[a]&theta.matrix[i,j]<ang.bin.cutoffs[a+1]){
        ang.bin.cell.counter.scramble[a,s]<-ang.bin.cell.counter.scramble[a,s]+1
        ang.bin.aggregated.signal.scramble[a,s]<-ang.bin.aggregated.signal.scramble[a,s]+I.for.analysis[i,j]

      }}}}

for (b in 1:r.bin.number){
  for (k in 1:length(fx)){
    for (l in 1: length(fy)){
      if(radial.matrix[k,l]>=r.bin.cutoffs[b]&radial.matrix[k,l]<r.bin.cutoffs[b+1]){
        r.bin.cell.counter.scramble[b,s]<-r.bin.cell.counter.scramble[b,s]+1
        r.bin.aggregated.signal.scramble[b,s]<-r.bin.aggregated.signal.scramble[b,s]+I.final[k,l]

      }}}}
}

#end of scramble#####################################################################

####Plotting the statistical results#########
####Angular Spectrum####
#this plot is to figure out how to adjust the y-axis -- write down the height of the highest peak
```

```
plot(ang.bins,ang.bin.averaged.signal,type="l")
ang.bin.averaged.signal.scramble <- ang.bin.aggregated.signal.scramble/ang.bin.cell.counter.scramble
matplot(ang.bins,ang.bin.averaged.signal.scramble,type="l",col="grey",lty = 1, ylim =
c(0.6,1.8),xlab="angular bins", ylab="averaged signal", main="Angual Spectrum AOI2")
lines(ang.bins,ang.bin.averaged.signal,type="l", col="red")
####Please save the plot as a PDF with an appropriate file name
#saving the output tables
angual.output<-cbind(ang.bins,ang.bin.averaged.signal,ang.bin.averaged.signal.scramble)
#give it a good name, do not forget the .csv extension
write.csv(angual.output, file="AOI2_angual_output.csv")

####Radial Spectrum##########
#this plot is to figure out how to adjust the y-axis, write down the height of the tallest peak
plot(r.bins,r.bin.averaged.signal,type="l")
r.bin.averaged.signal.scramble <- r.bin.aggregated.signal.scramble/r.bin.cell.counter.scramble
matplot(r.bins,r.bin.averaged.signal.scramble,type="l",col="grey",lty = 1, xlim=c(0,20), ylim = c(0,55),
xlab="radial bins", ylab="averaged signal", main="Radial Spectrum AOI2")
lines(r.bins,r.bin.averaged.signal,type="l", col="red")
#####Please save the plot as a PDF with an appropriate name

#saving the output tables
radial.output<-cbind(r.bins,r.bin.averaged.signal,r.bin.averaged.signal.scramble)
write.csv(radial.output, file = "AOI2_radial_output.csv")

#END#############################################################################
#################################################################################
```